Hindawi
International Journal of Chemical Engineering
Volume 2021, Article ID 4737513, 15 pages
https://doi.org/10.1155/2021/4737513

Research Article

Variation of the Number of Heat Sources in Methane Dry Reforming: A Computational Fluid Dynamics Study

Sunggeun Lee and Hankwon Lim

School of Energy and Chemical Engineering, Ulsan National Institute of Science and Technology, 50 UNIST-gil, Eonyang-eup, Ulju-gun, Ulsan 44919, Republic of Korea

Correspondence should be addressed to Hankwon Lim; hklim@unist.ac.kr

Received 12 August 2021; Revised 18 October 2021; Accepted 25 October 2021; Published 24 November 2021

Academic Editor: Achim Kienle

To overcome the weak point of the gas type heating (failure in heating uniformly and persistently), liquid type molten salt as a concentration of solar energy was considered as a heat source for dry reforming. This high-temperature molten salt flowing through the center of the tubular reactor supplies necessary heat. The dependence on the number of heat source of the hydrogen production was investigated under the assumption of the fixed volume of the catalyst bed. By changing these numbers, we numerically investigated the methane conversion and hydrogen flow rate to find the best performance. The results showed that the methane conversion performance and hydrogen flow rate improved in proportion to the number of heating tubes. For the one heat source, the reactor surrounded by a heat source rather than that located in the center is the best in terms of hydrogen yield. In addition, this study considered the case in which the system is divided into several smaller reactors of equal sizes and a constant amount of catalyst. In these reactors, we saw that the methane conversion and hydrogen flow rate were reduced. The results indicate that the installation of as many heating tubes as possible is preferable.

1. Introduction

Extensive use of hydrocarbons (fossil fuels) as an energy source has resulted in the global increase of temperatures and abnormal climate changes. Recent studies have pointed out that carbon dioxide and methane (more harmful than carbon dioxide) are the chief greenhouse gases. Both the reduction of these greenhouse emissions and the sufficient energy supply to the energy demands let one accelerate to find alternative energy sources. Hydrogen is an attractive candidate that satisfies these requirements. However, complete freedom from carbon emissions seems impossible, and the minimization of such emissions is a challenging problem.

There are many known ways to produce hydrogen: reforming, coal gasification, partial oxidation, and electrolysis. In reforming, there are also several fuels to reform, such as methane, ethanol, ammonia, and methanol. Among them, methane is widely used because it can be obtained naturally without much process as shale gas. The methane reforming method is categorized into several types: steam [1], dry (carbon dioxide) [2], partial oxidation [3], and autothermal reforming methods [4]. Methanol and biogas can also be used instead of methane. As for the methods, methane steam reforming is still the cheapest and most well-established reforming method despite its drawbacks, such as sintering and sulfur poisoning.

Dry or carbon dioxide reforming has gained considerable research attention as both greenhouse gases, namely, methane and carbon dioxide, are simultaneously reformed into syngas [5–36]. This method produces hydrogen and carbon monoxide with ratios between 1 and 2. However, the most important drawback of this reaction is the formation of coke on the catalyst, reducing its activity and thus requiring the regeneration of the catalyst to maintain its reaction performance. Nickel catalyst was used for methane steam reforming to study carbon deposition on catalyst. 600°C to 800°C temperature range, 0.5, 1.0, and 2.0 of steam to methane ratio, and pressure dependence were investigated. The increase of the pressure and the steam to methane ratio results in the decrease of carbon formation. 800°C and 0.5 steam to methane ratio gave the maximum carbon deposition [37]. Interesting removal of carbon deposits was reported [38] for mixed methane reforming and coke suppression by promoters [39]. Because the production of hydrogen is a highly endothermic reaction, an appropriate amount of heat is needed. This necessary heat is derived mostly from the combustion of natural gases, leading to another emission of greenhouse gases. As such, an alternative method is required to produce heat without the emission of greenhouse gases.

The sun is a well-known source of an enormous amount of energy. Almost all the energy that we use could be regarded as coming from the sun. Hence, effective and convenient methods have been developed to transfer solar energy: solar photochemical water splitting (artificial photosynthesis) and solar thermochemical water splitting using a parabolic, trough-type solar receiver [40–42]. In these developments, efficiency is important when one type of energy is transformed into another. For example, efforts to increase the efficiency of solar absorbers using coats of paint have been studied [43].

Another way of applying solar energy is to use it to power the reforming processes. Various types of solar reforming were reviewed like ASTERIX, directly irradiated annular pressurized receiver, and CAESER [44], which include reforming by using solar thermal energy [45–51]. A shell-type heat exchanger reactor that circulates heat using a molten salt stored in a tank is discussed for the reforming [52]. Molten salt is a means for storing solar energy as thermal energy. Another well-known method for storing solar energy is in the form of hydrogen formed by the electrochemical splitting of water, called photovoltaic water electrolysis. Studies about solar water splitting have also reported on high efficiency methods, such as 30% solar-to-hydrogen efficiency [53]. Although the temperature produced by concentrating solar energy is relatively high for reforming, an alternative reactor using a membrane can reduce the temperature, which is sufficient for a parabolic trough [54–59].

Other solar thermochemical applications for hydrogen production have also been reported [60–64]. Water splitting through concentrated solar energy with an oxygen-permeable membrane was analyzed [65]. To overcome the low-temperature gain in a parabolic trough, a membrane is applied. Studies have also conducted a CFD model analysis of a parabolic trough with a membrane reactor for molten salt reforming [66], especially for molten salt flowing over the outer surface as a heat source [67]. Some researchers have reviewed domestic and industrial applications of parabolic-trough-concentrating solar thermal collectors [68]. In the present model, the required heat was derived from solar energy, which is concentrated and stored in the molten salt.

This paper discusses the heat source geometry and its effect on methane conversion. As the heat source is a liquid rather than a gas, its property is easy and it has uniform supply of heat over long distances and its heat is long lasting. We investigated dry reforming because both potential greenhouse gases (methane and CO2) can be reformed simultaneously into useful syngas despite the possibility of coke formation, and this reaction has not yet been commercially developed. Section 2 presents the necessary equations and illustrates geometry of the reactor. With this information, the simulation results and discussions are provided in Section 3. The conclusions are presented in Section 4.

2. Numerical Methods: Governing Equations

In this section, we introduce the motivation for the study, schematic of the reactor, and mathematical background used for our simulation. Most equations have already been mentioned in literature [69]. The equations in this paper are limited to those required to help understand the present work.

As a renewable and sustainable option, solar energy is one of the most attractive sources of energy. In this study, we used molten salt as the heat source for reforming. Figure 1 shows the diagrammatic process starting from the source of the solar energy to the reforming reactor. In this study, the green-dashed-line box was the focus of our numerical analysis.

Figures 2(a) depicts the frontal view of the reactor, and Figures 2(b) and 2(c) display reactors with one heating tube at the center and an outer shell-type heat source, respectively. Our simulation investigates the methane conversion and hydrogen yield (flow rate) by varying the number of heating tubes and their positions. To maintain consistency, we fixed the total amount (volume) of the catalyst. That is, reducing the radius of the tubes is the only way to increase the number of tubes. The results will be compared with those obtained by placing a single heating tube at the center. There are two cases for a single heating tube depending on its location: the center and outer shell.

Figure 3 shows the frontal views of the three geometries simulated to which our numerical simulation was applied. We classify the geometries into three classes and denote them as 1, 2, and 3. In geometry 1, the number of the heating tubes varied from two to eight (note that seven is not available due to the irrational number: 360°/7). We studied the effect of changing the distance between the heating tubes (or in other words, the distance of heating tubes from the center of the reactor). Rotational symmetry along the cylinder axis was used in the construction of the geometry for convenience. A more general (without rotational symmetry) study might be appropriate for further study. The radius of the heating tubes becomes smaller as the number of tubes increases. In geometry 2, one of the heating tubes is located at the center of the reactor, while the remainder surrounds its center. The simulation was conducted by varying the distance between the heating tubes. In geometry 3, only the positions of the heating tubes marked by arrows were varied.

The reactor specifications, such as size and radius, are listed in Table 1.

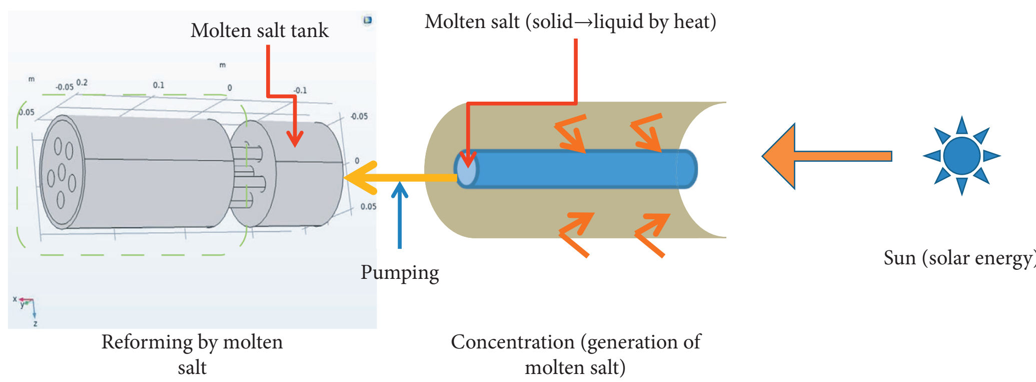

Figure 1: Conversion of solar energy to hydrogen. The green-dashed box is the focus of this study.

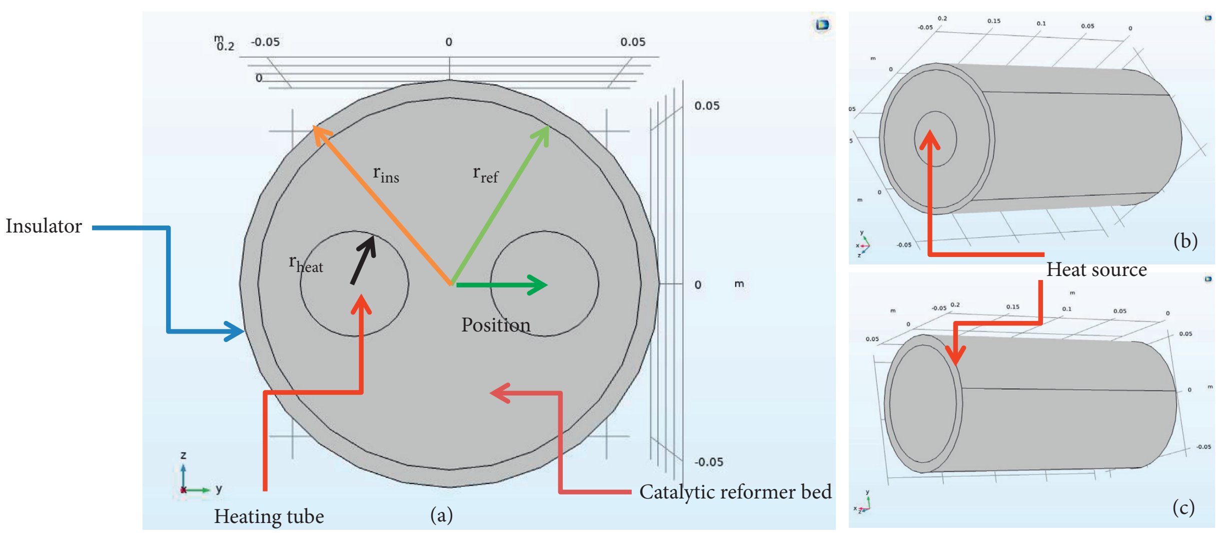

Figure 2: (a) Frontal view of the reactor and schematic of reactors with (b) one heating tube at the center and (c) outer shell-type heating.

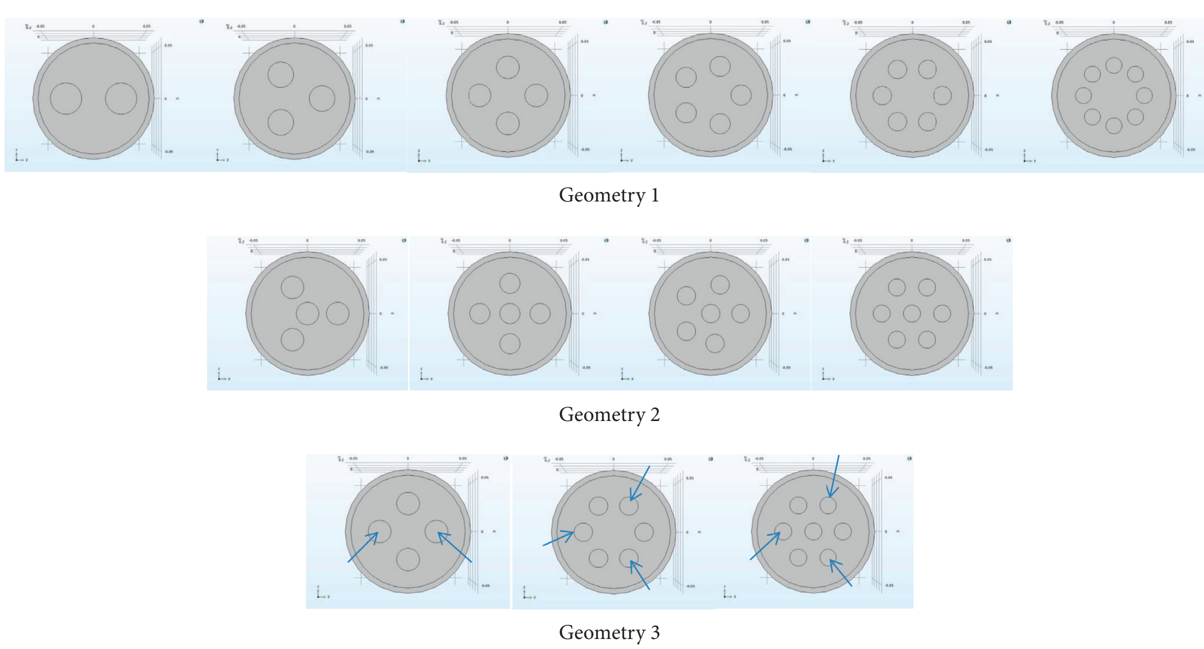

Figure 3: Frontal view of each reactor representing geometries 1, 2, and 3.

Table 1: Reactor specification.

Reactor length	0.2 m
Reactor radius	0.052 418 83 m
Heating tube radius	0.020 976 m (one), 0.014 83 m (two), 0.012 11 m (three), 0.010 488 m (four), 0.009 38 m (five), 0.008 563 m (six), 0.007 928 m (seven), 0.007 416 m (eight)
Thickness of insulator	0.005 m
Reactor radius for outer shell-type model	0.048 040 4m
Outer radius of shell-type model	0.0564 588 m (0.008 418 4 m thick)

The governing equations applied in this study are summarized as follows [69]. Note that the current study is focused on steady state only.

Heating tube is as follows.

Heat transport in the heating tube is formulated as

$$\nabla \cdot \left(-k_{ht}\nabla T\right) + \rho C_p \mathbf{u} \cdot \nabla T = 0. \tag{1}$$

The molten salt flows are described by the Navier–Stokes equations, that is, (2) and (3). In this flow, laminar flow is assumed without loss of consistency:

$$\boldsymbol{\rho}(\mathbf{u}\cdot\nabla)\mathbf{u} = \nabla \cdot \left[-p\mathbf{I} + \mu\left(\nabla\mathbf{u} + (\nabla\mathbf{u})^T\right) - \frac{2\eta}{3}\,(\nabla\cdot\mathbf{u})\,\mathbf{I}\right], \tag{2}$$

$$\nabla \cdot (\rho\mathbf{u}) = 0. \tag{3}$$

The reaction is highly endothermic and needs an insulating jacket to reduce the heat loss. The reactor covered by such an insulator satisfies the following:

$$\nabla \cdot \left(-k_i \nabla T\right) = 0. \tag{4}$$

Reformer bed is as follows.

The behavior of the porous media is usually described by the Ergun equation [70], which is well suited to experiments for both low and high Reynolds numbers. In the present simulation, we applied a low Reynolds number by assumption, and the flow was described through Darcy's law, according to which the velocity and pressure satisfy the following relation:

$$\mathbf{u} = -\frac{\kappa_{ref}}{\mu_{ref}}\,\nabla p. \tag{5}$$

The equation of continuity is derived as follows:

$$\nabla \cdot (\rho\mathbf{u}) = Q_m. \tag{6}$$

The reformer bed satisfies heat capacity given by

$$\epsilon_{ref}\left(\rho C_p\right)_f + \left(1-\epsilon_{ref}\right)\left(\rho C_p\right)_s = 0, \tag{7}$$

where subscripts f and s represent the discriminate fluid and solid, respectively.

The thermodynamic law describing the reformer bed is given as

$$\nabla \cdot \left(-k_{ref}\nabla T_{ref}\right) + \left(\rho C_p\right)_f \mathbf{u}\cdot\nabla T_{ref} = Q. \tag{8}$$

Heat exchange occurs during the reaction, and heat generation Q is given by $r\Delta H_r$. A heat source with reaction rates r_1 and r_2 and the corresponding enthalpies H_1 and H_2 satisfy

$$\nabla \cdot \left(-k_{ref}\nabla T_{ref}\right) + \left(\rho C_p\right)_f \mathbf{u}\cdot\nabla T_{ref} = -r_2 \cdot H_1 - r_2 \cdot H_2. \tag{9}$$

The diffusion of species satisfies the Maxwell–Stefan diffusion equation [70]. Inside the reformer filled with the catalyst, the diffusion is described as

$$\rho(\mathbf{v}\cdot\nabla)\omega_i + \nabla\cdot\left(-\rho\omega_i\sum_{j=1}^{n} D_{ij}\left(\nabla x_j + \left(x_j-\omega_j\right)\left(\frac{\nabla p}{p}\right)\right) - D_i^T\left(\frac{\nabla T}{T}\right)\right) = R_i, \tag{10}$$

where x_i is the mole fraction for species i and is formulated as $x_i = (\omega_j/M_j)\,(\sum(\omega_j/M_j))^{-1}$. The thermal diffusion coefficients are denoted by D_i^T, and the source term for each species is represented by R_i. The coefficients D_{ij} represent the binary diffusion coefficients [70] depending on σ_{ij} and $\Omega_{D_{ij}}$. Here, σ_{ij} is the spherical molecule Lennard–Jones diameter of the spherical molecule and $\Omega_{D_{ij}}$ is the collisional integral, which is dimensionless for molecular diffusion. Binary coefficients are explicitly formulated as

$$D_{ij} = 0.001\,858\,3\sqrt{T^3\left(\frac{1}{M_i}+\frac{1}{M_j}\right)}\frac{1}{p\,\sigma_{ij}^2\Omega_{D_{ij}}}, \quad (11)$$

where M_i is the molecular weight of the species and D_{ij} is temperature dependent; nevertheless, we assumed that these values are constant and calculated at 800 K. The above-mentioned source term is given by $R_i = -r_1 M_{CH_4} + 2r_1 M_{H_2} - r_2 M_{H_2} - r_1 M_{CO_2} - r_2 M_{CO_2} + 2r_2 M_{CO} + r_2 M_{CO}$. The convective flux is expressed as follows at the outlet:

$$\mathbf{n}\cdot\left(-\rho\omega_i\sum_{j=1}^{n} D_{ij}\left(\nabla x_j + \left(x_j - \omega_j\right)\frac{\nabla p}{p}\right) - D^T\frac{\nabla T}{T}\right) = 0. \quad (12)$$

The lists of parameters used in numerical simulation are summarized in Table 2 [69].

COMSOL Multiphysics 5.5 is used for solving these equations.

2.1. Reaction: Methane Dry (CO_2) Reforming. In this study, we considered methane dry reforming, which may be expressed as follows [72]:

$$CH_4 + CO_2 \longrightarrow 2CO + 2H_2,\ \Delta H = 247.3\,kJ\,mol^{-1}$$
$$r_1 = k_1\cdot\left[\frac{K_{CO2}K_{CH4}P_{CO2}P_{CH4}}{\left(1 + K_{CO2}P_{CO2} + K_{CH4}P_{CH4}\right)^2}\right]\cdot\left[1 - \frac{\left(P_{CO}P_{H2}\right)^2}{K_1 P_{CH4}P_{CO2}}\right], \quad (13)$$

$$CO_2 + H_2 \longrightarrow CO + H_2O,\ \Delta H = 41\,kJ\,mol^{-1}$$
$$r_2 = k_2 P_{CO2}\cdot\left[1 - \frac{P_{CO}P_{H2O}}{K_2 P_{CO2}P_{H2}}\right]. \quad (14)$$

Rhodium catalyst, 0.5 wt.-% Rh/Al2O3 catalyst, was used for the range 600°C–800°C. The rhodium catalyst was selected because no carbon formation was shown and the deactivation of rhodium catalyst decreases as temperature increases.

Here, k1 and k2 are the rate constants for each reaction, and KCO2, KCH4, K1, and K2 are the equilibrium constants. They are explicitly written as follows:

$$K_{CO_2} = 2.64\times10^{-7}e^{376.41\left[J\cdot mol^{-1}\right]1/RT}\left[Pa^{-1}\right]$$
$$K_{CH_4} = 2.63\times10^{-7}e^{406.84\left[J\cdot mol^{-1}\right]1/RT}\left[Pa^{-1}\right]$$
$$k_1 = 6.45\times10^{6}\,e^{-102.065\left[J\cdot mol^{-1}\right]1/RT}\left[mol\cdot s^{-1}\cdot m^{-3}\right]$$
$$k_2 = 9.28\times10^{-2}e^{-731.05\left[J\cdot mol^{-1}\right]1/RT}\left[mol\cdot s^{-1}\cdot Pa^{-1}\cdot m^{-3}\right]$$
$$K_1 = 10^{10}\times e^{34.011}\cdot e^{-258.598\left[J\cdot mol^{-1}\right]1/RT}\left[Pa^2\right]$$
$$K_2 = 68.78e^{-37\,500.3\left[J\cdot mol^{-1}\right]1/RT} \quad (15)$$

3. Results and Discussions

We investigated the effect of the geometry of the heating tube on methane dry reforming while maintaining a fixed total volume of the catalyst or heating tube. Thus, the radius of the heating tube decreases with the increase in the number of heating tubes. We attempted to arrange the heating tubes as symmetrically as possible and identified the designs that offer good methane convergence. The effect of the placement of the heating tubes in more general positions is of particular interest.

The following is a comment about model validation and mesh independence. Before presenting the results and discussion, we briefly comment on the model validation and grid mesh independence of our model. As our simulation is based on a previous study [69], which has discussed these two steps, we have omitted these procedures.

The temperature distribution of the reactor for geometry 1 is shown in Figure 4. In a previous study [73], we determined the counter-current flow (the flow directions of heat and feedstocks are opposite) to be more relevant by comparing the methane conversion between the cocurrent and counter-current flow of the heating tube. Therefore, in the present study, we considered only the counter-current flow. A darker red color shows a higher temperature than the lighter red or blue color.

Table 2: Parameters used in numerical studies.

Parameters in the equations		
$u_{in,ht}$	$1\ \mathrm{m\cdot s^{-1}}$	Heating tube inlet velocity
$T_{in,ht}$	1000 K	Heating tube inlet temperature
$p_{in,ref}$	75 Pa	Reformer bed inlet pressure
p_{ref}	1.0×10^5 Pa	Reference pressure
$T_{in,ref}$	800 K	Reformer bed inlet temperature
h_{ht}	$100\,W\cdot m^{-2}\cdot \mathrm{K}^{-1}$	Heat transfer coefficient[a] (heating tube)
h_j	$1\,W\cdot m^{-2}\cdot \mathrm{K}^{-1}$	Heat transfer coefficient[b] (insulating jacket)
Binary diffusion coefficients (800 K), Lee et al. [69, 71]		
$\omega_{CH_4,in}$	0.15	Weight fractions
$\omega_{H_2,in}$	0.005	Weight fractions
$\omega_{CO,in}$	0.000 01	Weight fractions
$\omega_{CO_2,in}$	0.42	Weight fractions
$\omega_{Ar,in}$	0.429 99	Weight fractions
ρ_j	$24\ \mathrm{kg\cdot m^3}$	Density[a]
$C_{p,j}$	$1.9\ \mathrm{J\cdot kg^{-1}\cdot K^{-1}}$	Heat capacity[a] of insulating jacket
k_j	$0.027\ \mathrm{W\cdot m^{-1}\cdot K^{-1}}$	Thermal conductivity[a]
$C_{p,ref}$	$280\,0\ \mathrm{J\cdot kg^{-1}\cdot K^{-1}}$	Heat capacity[b]
k_{ref}	$0.1\ \mathrm{W\cdot m^{-1}\cdot K^{-1}}$	Thermal conductivity[b]
μ_b	$2.7 \times 10^{-5}\ \mathrm{Pa\cdot s}$	Viscosity[c] of reformer bed
ϵ_{ref}	0.25	Porosity
κ_{ref}	$1.0 \times 10^{-9}\ \mathrm{m^2}$	Permeability[d]
H_1	$247 \times 10^3\ \mathrm{J\cdot mol^{-1}}$	Enthalpy of reaction 1
H_2	$412 \times 10^2\ \mathrm{J\cdot mol^{-1}}$	Enthalpy of reaction 2

[a]We considered this value; for various values, see https://www.engineeringtoolbox.com/thermal-conductivity-d_429.html and for polyurethane foam, https://www.nuclear-power.net/nuclear-engineering/heat-transfer/heat-losses/insulation-materials/polyurethane-foam/. [b]https://www.engineeringtoolbox.com/specific-heat-capacity-d_391.html, [c]https://www.engineeringtoolbox.com/gases-absolute-dynamic-viscosity-d_1888.html, and [d]https://tel.archives-ouvertes.fr/tel-00848600/document.

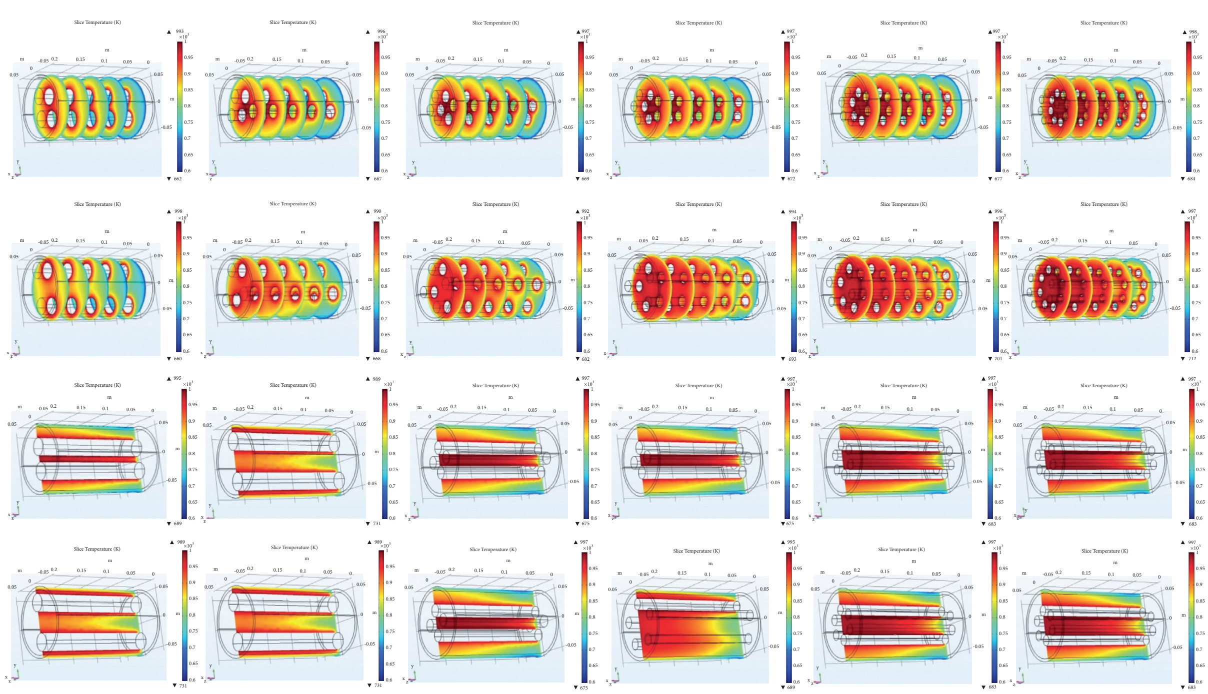

Figure 4: Temperature distributions (sliced perpendicular (first and second line) and parallel (third and fourth line) to the axis) according to the number of heating tubes for geometry 1: the cases in which the distance between the heating tubes is closest (first and third line) and farthest (second and fourth line).

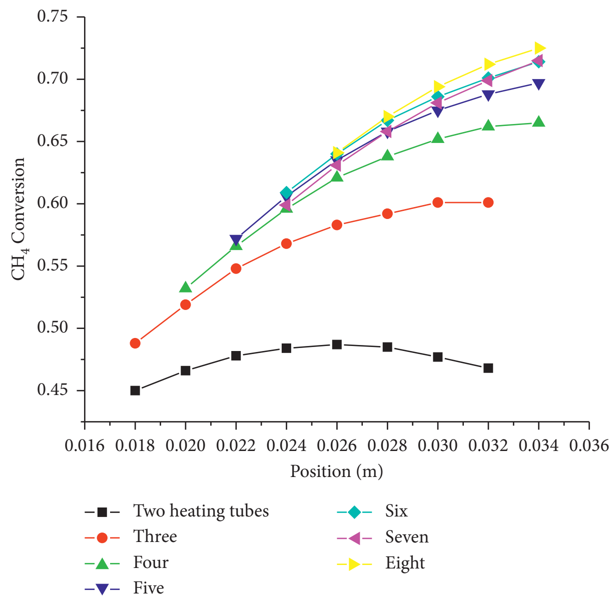

FIGURE 5: CH4 conversions for different heating tube configurations.

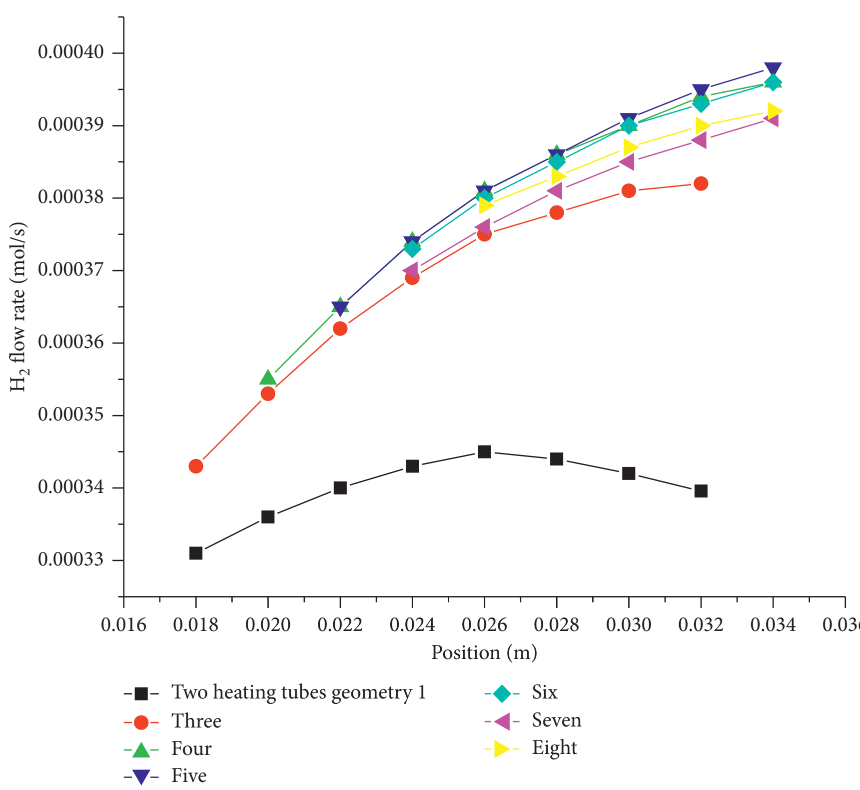

FIGURE 6: H2 flow rate according to the number of heating tubes.

As mentioned earlier, dry reforming is an endothermic reaction and requires a high temperature. As the area increases, the temperature volume increases (as the darker red region becomes darker) and the reaction becomes more violent than the adjacent lower temperature region. The figure shows that the darker red colored region increases in area as the number of heating tubes increases (to the right direction in the figure), and the heating tubes are located farther from the center (down the figure). Thermodynamically, uniformly distributed high temperatures (without much temperature gradient) promote better performance of the reactor. To achieve this, the geometrically optimized heat supply of the reactor must be determined. Figure 4 indicates the conversion of methane and flow rate of hydrogen.

The conversion of methane according to the number of heating tubes in geometry 1 is shown in Figure 5. Here, the

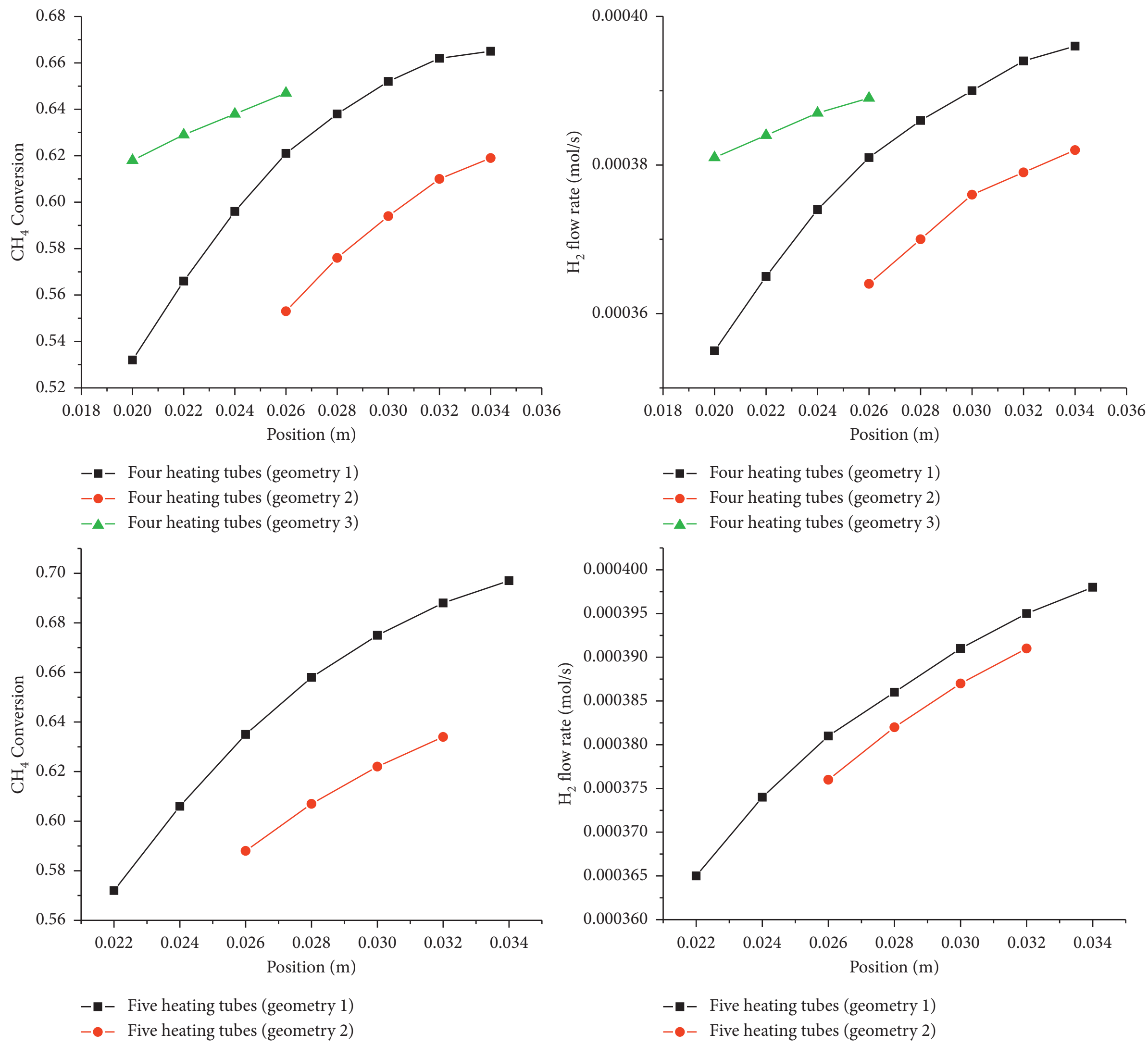

(a)

Figure 7: Continued.

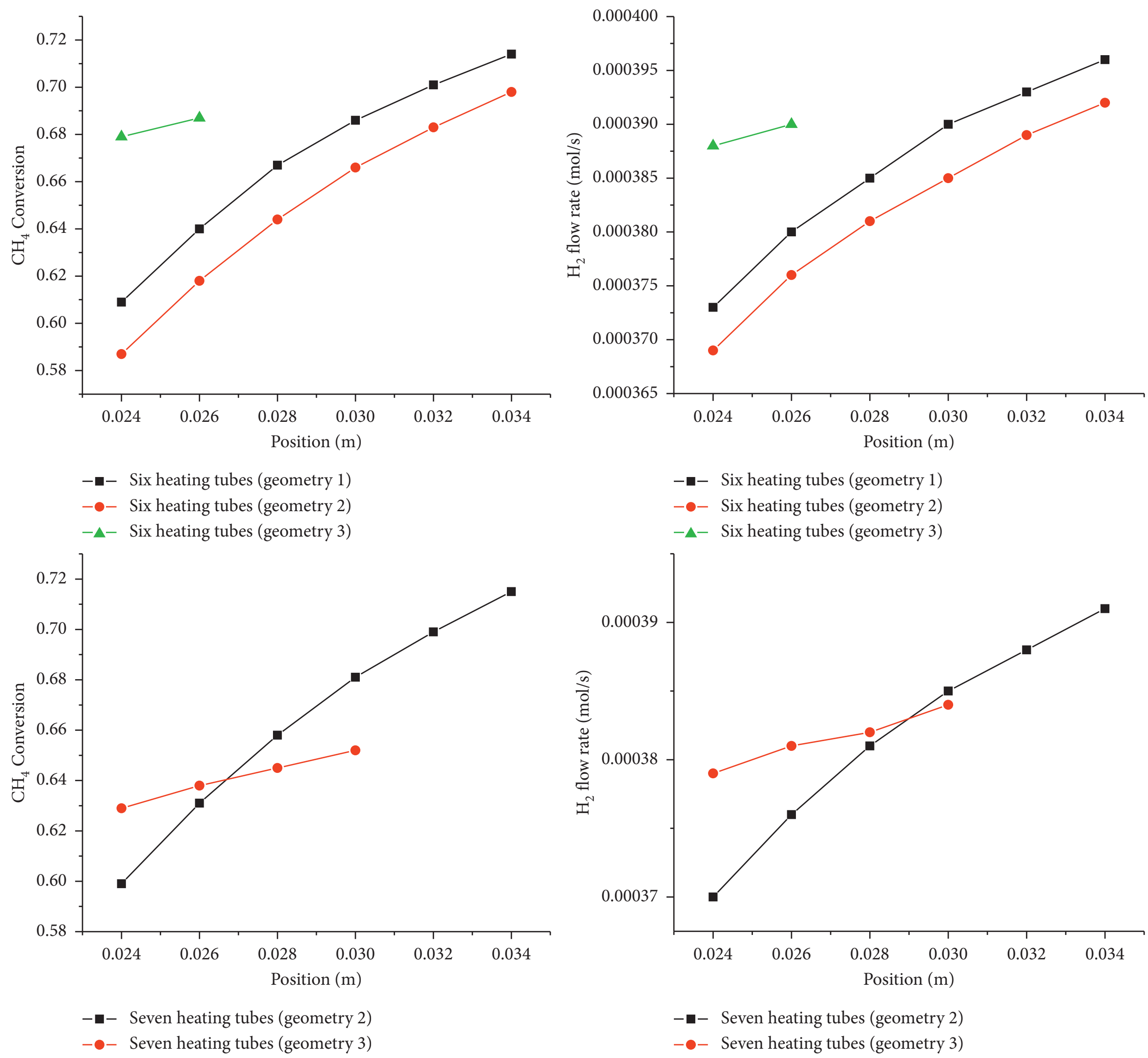

(b)

Figure 7: CH4 conversion and H2 flow rates with varying the number of heating tubes: the number of heating tubes increases from top to bottom (4, 5, 6, and 7) for each geometry.

positions mean the distance between the centerlines of both inner and outer cylinders. Subsequent positions are determined by increasing the distance between the heating tubes or the distance from the center. First, the overall methane conversion is proportional to the number of heating tubes. In each case, however, the rate of increase is different. For a smaller number of heating tubes, the rate of increase decreases as the position of the heating tubes from each other increases. A two-heating-tube configuration has a turning point where the conversion of methane peaks and subsequently decreases.

The hydrogen yield/flow rate has almost the same behavior as methane conversion, as shown in Figure 6.

Figure 3 shows two or three types of geometries for a given number of heating tubes. Because of the computational limitations due to error, the full range of data for geometry 1 is not yet available. Figure 7 shows the methane conversion and hydrogen flow rates in these geometries. In the case of four heating tubes, geometry 3 showed the highest methane conversion and hydrogen flow rate at the common position of 0.026 m. However, the results in Figures 5 and 6, which display a lower rate of increase, show that geometry 1 yields the highest performance. Geometry 2 showed the lowest performance among the three geometries. Such patterns apply to all the scenarios depicted in Figure 7.

In Figure 7, both the methane conversion and hydrogen flow rate for each geometry increase as the number of heating tubes does. Moreover, both of them in geometry 3 are the highest for almost all of the cases and followed by geometry 1 and geometry 2 in turn. We see that the flow rate and the conversion grow as the position becomes large. This means that the performance becomes increased as the heating tubes become farther from the center within our simulation. However, we see that for the same distance, for example, 0.024 m, the conversion increases as the number of heating tubes but decreases for 7 numbers of heating tubes.

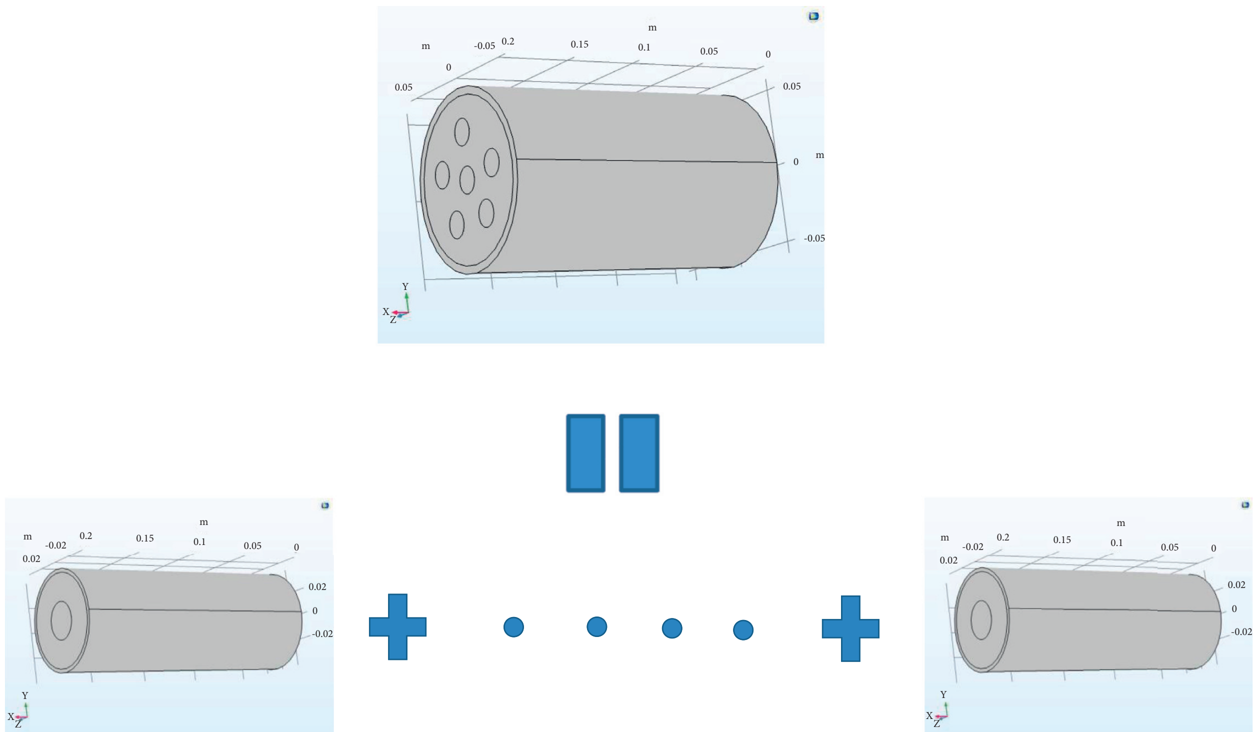

Figure 8: One reactor with a number of heating tubes is divided into the same number of reactors with one heating tube with an equal amount of catalyst.

These results can be compared to the results for a single heating tube. This case can be divided into two cases: the one case in which the heat source is located along the center and the other case in which the reactor is surrounded by a shell-type heat source. The numerical analysis of methane conversion for a single heating tube through the center is approximately 34.8% and the hydrogen flow rate is approximately 2.8857×10^{-4} mol/s. This is the lowest value obtained in this study. The methane conversion rate obtained when heat was supplied from the outer surface was 69.95%, and the hydrogen flow rate was 4.1165×10^{-4} mol/s. The methane conversion rate of the outer shell heat source corresponds to the case where the distance was 0.032 m; however, the hydrogen flow rate of the outer shell-type heat source surpasses all the above-mentioned results. We applied the same amount of heat and catalyst for the outer shell-type heat source, effectively reducing the reactor size and leading to a more enhanced hydrogen flow rate.

Let us consider the average velocity of the molten salt in each geometry. As demonstrated earlier, the radius of the heating tube decreases as the number of heating tubes increases. However, the average velocity of flow remains the same for all the studied cases. This may be due to the fact that the reactor tube in the study is too short for the velocity difference to discriminate manifestly.

Hydrogen permeation membranes are used in the process in order to lower the temperature and separate the hydrogen. However, the scope of our study was limited to the geometrical variations. It remains to be determined where to place the membrane and which type of membrane we use.

In another view of the problem, a reactor was divided into several smaller, separated reactors, and each reactor had one heating tube. Figure 8 displays the concept of the separated reactors. When the reactor size needs to be reduced, it can be done by dividing one reactor into smaller units. There are many ways to develop this idea by considering the arrangement of the heat source. For instance, five types are shown in Figure 9, applicable to six reformers. Among them, the most practicable is shown in Figure 9(a), and this design of the heat source gives the most uniform heat distribution to all reactors with the least heat loss. Moreover, it is the most compact size, for both the given space and the given number of reactors.

Owing to the many advantages of the reactor shown in Figure 9(a), we applied that type of heat source to the following reformer. Figure 10 shows two types of reactors. Figure 10(a) (especially the green-dashed box) was studied in the previous segment, and Figure 10(b) is a new design based on the results indicated in Figure 9. The reactor in Figure 10(a) is divided into smaller reactors (shown in Figure 10(b) inside the dark dashed green box), keeping the catalysis volume and number of heating tubes constant.

The methane conversion and hydrogen flow rate for Figure 10(b) are shown in Figure 11. Compared with Figure 5, Figure 11 shows that the conversion and flow rates are similar to the case of which distance of the tubes is 0.024 m. Therefore, this type of reactor performs worse than a single reactor with a varying number of heating tubes does.

Molten salt can be used as a heat source in fluidized bed type (uniform mixing and temperature gradients but large reactor scale) or bubble column reactor (high heat and

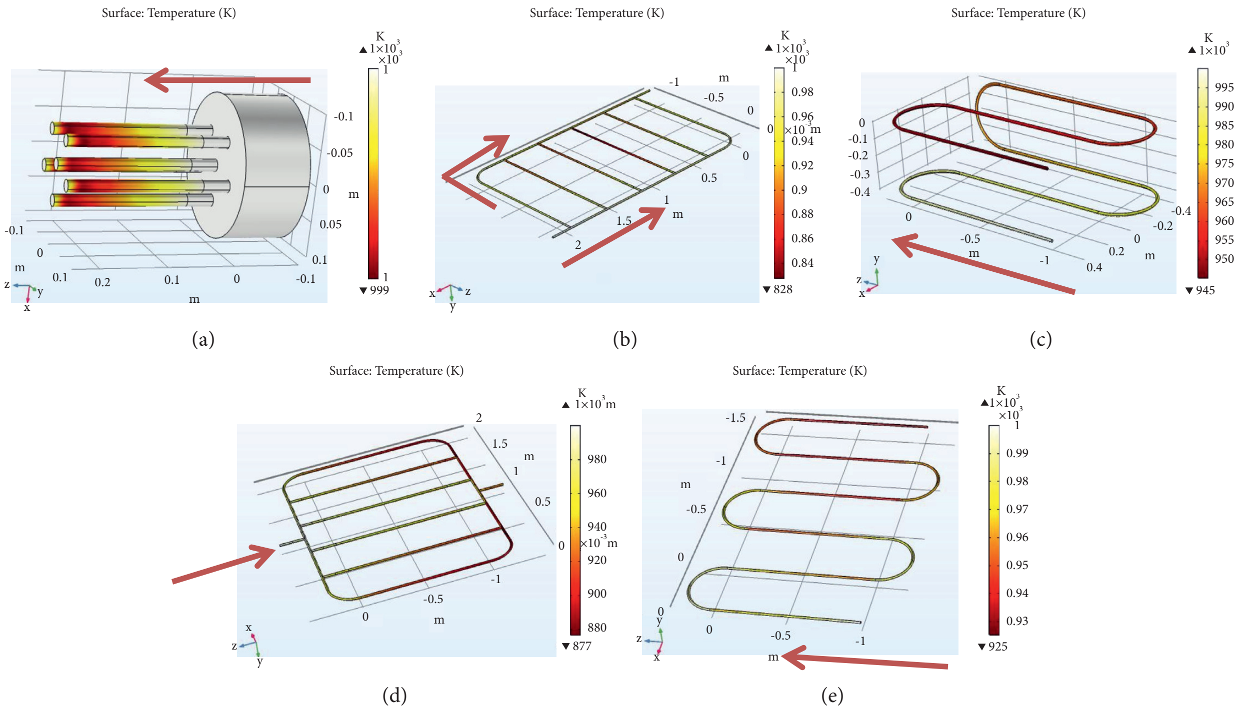

FIGURE 9: Heat source configurations for the realization of Figure 8. The arrows indicate the flow direction.

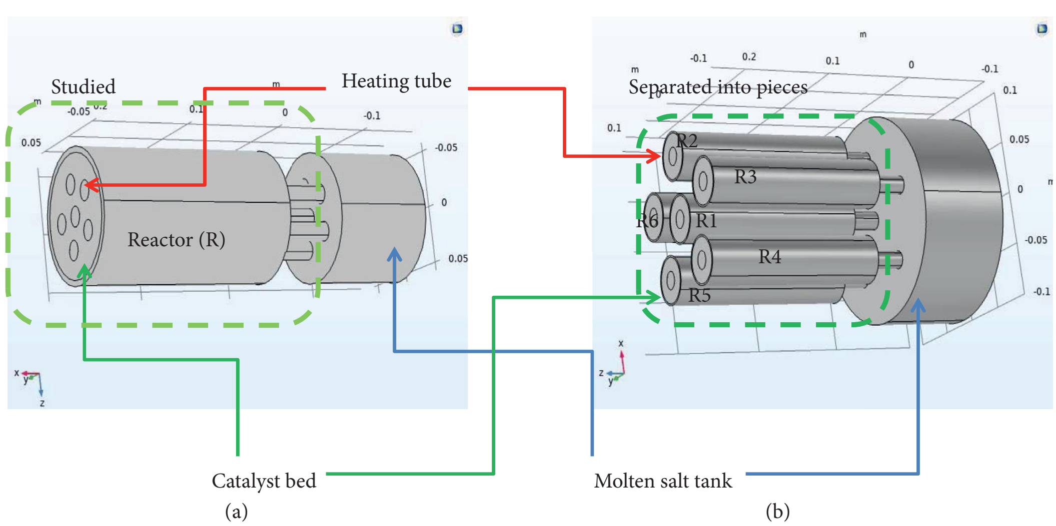

FIGURE 10: Realization of Figure 8 (especially dark dashed green box in Figure 10(b)) for six reactors based on the heat analysis results of Figure 9. Green-dashed box in (A) was studied in detail in this manuscript.

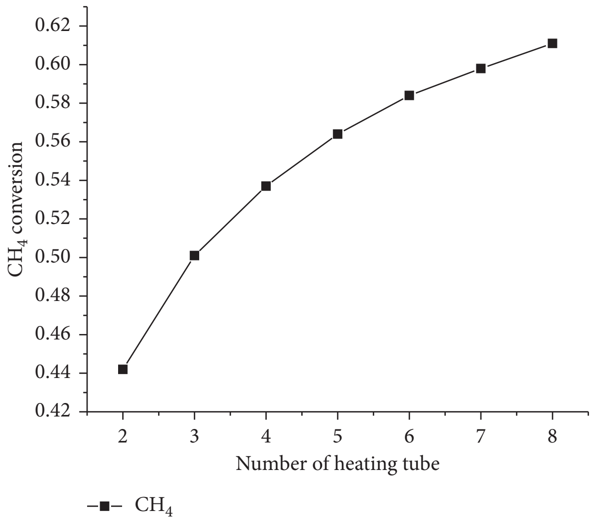

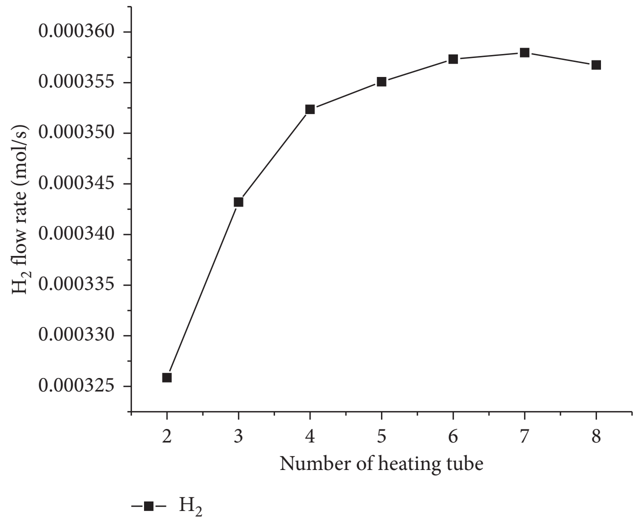

Figure 11: Methane conversion (left) and hydrogen flow rate (right).

mass transfer). Our model, however, compared to these two reactors (which is not well understood due to complexity of reaction), is more tractable in that our model can be constructed in smaller reactor scale which raises heat transfer and more well-known reaction. Especially, our reactor overcomes gas type heat source using liquid (molten salt) because liquid has higher heat capacity and carries longer distance than gas. Our reactor is a collection of advantages of fluidized bed or column reactor and packed bed reactor.

Interesting experimental and CFD study was investigated for the pressure drop of the packed bed reactor [7]. The reactor is filled with porous catalysts particle with pore size ranging from 0.2 mm to 2.0 mm. The increase of the pore size from 0.2 mm to 2.0 mm results in decreasing of the pressure drop by more than 3 times. In (1) in [7], we expect that large porosity approximation leads to v^2 dependence in Δp and vice versa. In our simulation, we fixed the inlet and outlet pressure as a boundary condition shown in the table and simplified the fluid motion without catalysts structure. It would be interesting if we use velocity boundary condition instead of pressure one to study pressure drop.

4. Conclusions

In a reactor, the maintaining of a uniform high-temperature distribution is important for high methane conversion and hydrogen yield rates. Because of its highly endothermic nature, natural gas reforming for the generation of hydrogen requires heat. Compared to the gas, the liquid has larger specific heat capacity than the gas does. Then, the liquid heat source is superior to the gas one in that it heats up the reactor longer and more uniformly. This property makes it possible to design various reactors from small in sizes to their complicated structures as illustrated in the manuscript. We might expect that this improves the performance of the packed bed reactor for various designs.

In this study, we used a liquid (molten salt) as the heat source because it has several advantageous over gaseous sources. The total mass of the heated molten salt in each model was kept unvaried (by keeping the total volume constant) while the number of heating tubes varied. The results indicate that it is better to divide the heat source as much as possible and distribute them uniformly inside the reactor to transfer heat uniformly.

With the help of commercial COMSOL Multiphysics 5.5 software, we numerically verified that both the methane conversion and hydrogen flow rate are proportional to the number of heating tubes. For one heating tube, the reactor surrounded by the heat source surpasses all the reactors studied in the hydrogen yield.

In addition, we considered dividing the reactor into smaller reactors, each with a heating tube, and the total sum of the catalyst in each reactor was equal to that before division. In this case, the methane conversion and hydrogen flow rate corresponded to the results of the reactor before division, in which the heating tubes are separated from each other by a particular distance. However, the overall performance of the separated reactors is lower than that of the one integrated reactor.

Therefore, considering both the methane conversion and hydrogen yield, we suggest that installing as many heating tubes as possible is preferable when using liquid (molten salt) as the heat source in a packed bed reactor rather than separating the reactors into many pieces, even though the reactor surrounded by the heat source is the best in terms of hydrogen yield.

4.1. Summarizing

(i) We used COMSOL Multiphysics to study a packed bed reactor of methane dry reforming with liquid heat source-molten salt. Replacing the gas type heat source by liquid molten salt brought together the advantages in fluidized bed or bubble column reactors having high heat transfer and packed bed reactor well understood. This liquid type heat source makes it possible to construct reactor in small scale. Using solar energy as a heat source gives us almost free of CO2 emission compared to gas type heat source.

(ii) Hydrogen production is proportional to the number of heating tube while the outer shell-type heating is better for one heating tube.

(iii) Occurrence of catalysts fowling forbids continuous working of reactor. There is a limitation in heat transfer compared to the fluidized bed. Changing the shape of the reactor, for example, like frustum of cone shape reactor with frustum heating tubes and finding best performance, would be an interesting study. Shell-type heating will be a good challenge because we have seen in this work that outer shell heating is best for one heating tube case. In addition, methane pyrolysis in packed bed type would be a future study for the application of reactor.

Nomenclature

T: Temperature, K
p: Pressure, Pa
h: Coefficient of heat transfer, $W \cdot K^{-1}$
u_{ht}: Velocity of heating tube, $m \cdot s^{-1}$
M_i: Molar mass, $kg \cdot mol^{-1}$
D_{ij}: Binary diffusion coefficient, $m^2 \cdot s^{-1}$
κ_{ref}: Permeability, m^2
ρ_j: Density of insulator, $kg \cdot m^{-3}$
$C_{p,j}$: Heat capacity, $J \cdot kg^{-1} \cdot K^{-1}$
k_j: Thermal conductivity, $W \cdot m^{-1} \cdot K^{-1}$
$\omega_{i,in}$: Initial weight fraction, dimensionless
μ_b: Viscosity (reformer bed)
Q_m: Mass source, $kg \cdot m^{-3} \cdot s^{-1}$
ϵ_{ref}: Porosity, dimensionless
H_i: Enthalpy, $J \cdot mol^{-1}$
r_i: Reaction rate, $mol \cdot s^{-1} \cdot m^{-3}$
k_i: Rate coefficient, $mol \cdot s^{-1} \cdot m^3$
K_1: Equilibrium constant, $kg^2 \cdot s^{-2} \cdot m^{-4}$
K_2: Equilibrium constant, dimensionless.

Data Availability

The data used to support the findings of this study are included within the supplementary information file.

Conflicts of Interest

The authors declare that there are no conflicts of interest regarding the publication of this paper.

Acknowledgments

This work was supported by the National Research Foundation of Korea (NRF) grant funded by the Korea government (NRF- 2019M1A2A2065614) and also supported by the 2021 Research Fund (1.210103.01) of UNIST (Ulsan National Institute of Science and Technology).

Supplementary Materials

This section includes data for molten salt-number of heating tube. (*Supplementary Materials*)

References

[1] J. R. Rostrup-Nielsen, *Catalytic Steam Reforming*, Springer, Heidelberg, Berlin, 1984.

[2] J. H. Edwards and A. M. Maitra, "The chemistry of methane reforming with carbon dioxide and its current and potential applications," *Fuel Processing Technology*, vol. 42, no. 2-3, pp. 269–289, 1995.

[3] M. Fathi, E. Bjorgum, T. Viig, and O. A. Rokstad, "Partial oxidation of methane to synthesis gas:," *Catalysis Today*, vol. 63, no. 2-4, pp. 489–497, 2000.

[4] S. Ayabe, H. Omoto, T. Utaka et al., "Catalytic autothermal reforming of methane and propane over supported metal catalysts," *Applied Catalysis A: General*, vol. 241, no. 1-2, pp. 261–269, 2003.

[5] J. Shen, A. A. C. Reule, and N. Semagina, "Ni/MgAl2O4 catalyst for low-temperature oxidative dry methane reforming with CO2," *International Journal of Hydrogen Energy*, vol. 44, no. 10, pp. 4616–4629, 2019.

[6] ö. Aydin, A. Kubota, D. L. Tran, M. Sakamoto, and Y. Shiratori, "Performance and durability of one-cell module of biogas-utilizing SOFC equipped with graded indirect internal reformer," *International Journal of Hydrogen Energy*, vol. 43, p. 17431, 2018.

[7] D. Pashchenko, I. Karpilov, and P. Mustafin, "Numerical calculation with experimental validation of pressure drop in a fixed-bed reactor filled with the porous elements," *AIChE Journal*, vol. 66, Article ID e16937, 2020.

[8] A. Tran, A. Aguirre, H. Durand, M. Crose, and P. D. Christofides, "CFD modeling of a industrial-scale steam methane reforming furnace," *Chemical Engineering Science*, vol. 171, pp. 576–598, 2017.

[9] K. Phuakpunk, B. Chalermsinsuwan, S. Putivisutisak, and S. Assabumrungrat, "Parametric study of hydrogen production via sorption enhanced steam methane reforming in a circulating fluidized bed riser," *Chemical Engineering Science*, vol. 192, pp. 1041–1057, 2018.

[10] C. Sarno, I. Luisetto, F. Zurlo, S. Licoccia, and E. Di Bartolomeo, "Lanthanum chromite based composite anodes for dry reforming of methane," *International Journal of Hydrogen Energy*, vol. 43, no. 31, pp. 14742–14750, 2018.

[11] L. Tartakovsky and M. Sheintuch, "Fuel reforming in internal combustion engines," *Progress in Energy and Combustion Science*, vol. 67, pp. 88–114, 2018.

[12] M. A. Soria, C. Rocha, S. Tosti, A. Mendes, and L. M. Madeira, "COx free hydrogen production through water-gas shift reaction in different hybrid multifunctional reactors," *Chemical Engineering Journal*, vol. 356, pp. 727–736, 2019.

[13] E. Garía-Díez, F. García-Labiano, L. F. de Diego et al., "Calcium-looping for post-combustion CO2 capture. On the adverse effect of sorbent regeneration under CO2," *Chemical Engineering Journal*, vol. 325, p. 369, 2017.

[14] F. Mesrar, M. Kacimi, L. F. Liotta, F. Puleo, and M. Ziyad, "Syngas production from dry reforming of methane over ni/perlite catalysts: effect of zirconia and ceria impregnation," *International Journal of Hydrogen Energy*, vol. 43, no. 36, pp. 17142–17155, 2018.

[15] C.-H. Liao and R.-F. Horng, "Experimental study of syngas production from methane dry reforming with heat recovery

strategy," *International Journal of Hydrogen Energy*, vol. 42, no. 40, pp. 25213–25224, 2017.

[16] C. Gaber, M. Demuth, R. Prieler, C. Schluckner, and C. Hochenauer, "An experimental study of a thermochemical regeneration waste heat recovery process using a reformer unit," *Energy*, vol. 155, pp. 381–391, 2018.

[17] Y. Benguerba, M. Virginie, C. Dumas, and B. Ernst, "Computational fluid dynamics study of the dry reforming of methane over Ni/Al2O3 catalyst in a membrane reactor. Coke deposition," *Kinetics and Catalysis*, vol. 58, no. 3, pp. 328–338, 2017.

[18] J. N. Heo, N. Son, J. Shin, J. Y. DO, and M. Kang, "Efficient hydrogen production by low-temperature steam reforming of propane using catalysts with very small amounts of Pt loaded on NiMn2O4 particles," *International Journal of Hydrogen Energy*, vol. 45, no. 41, pp. 20904–20921, 2020.

[19] D. Mallick, P. Mahanta, and V. S. Moholkar, "Co-gasification of coal and biomass blends: chemistry and engineering," *Fuel*, vol. 204, pp. 106–128, 2017.

[20] S. S. Itkulova, Y. Y. Nurmakanov, S. K. Kussanova, and Y. A. Boleubayev, "Production of a hydrogen-enriched syngas by combined CO2-steam reforming of methane over Co-based catalysts supported on alumina modified with zirconia," *Catalysis Today*, vol. 299, pp. 272–279, 2018.

[21] S. Akbari-Emadabadi, M. R. Rahimpour, A. Hafizi, and P. Keshavarz, "Production of hydrogen-rich syngas using Zr modified Ca-Co bifunctional catalyst-sorbent in chemical looping steam methane reforming," *Applied Energy*, vol. 206, pp. 51–62, 2017.

[22] A. Tran, M. Pont, M. Crose, and P. D. Christofides, "Real-time furnace balancing of steam methane reforming furnaces," *Chemical Engineering Research and Design*, vol. 134, pp. 238–256, 2018.

[23] I. Aloisi, A. Di Giuliano, A. Di Carlo, P. U. Foscolo, C. Courson, and K. Gallucci, "Sorption enhanced catalytic Steam Methane Reforming: experimental data and simulations describing the behaviour of bi-functional particles," *Chemical Engineering Journal*, vol. 314, pp. 570–582, 2017.

[24] G. M. Karthik and V. V. Buwa, "Effect of particle shape on fluid flow and heat transfer for methane steam reforming reactions in a packed bed," *AIChE Journal*, vol. 63, no. 1, pp. 366–377, 2017.

[25] A. K. Rohini, S. H. Choi, and H. J. Lee, "Numerical parametric study on the burner arrangement design for hydrogen production in a steam methane reformer," *International Journal of Energy Research*, vol. 45, no. 11, pp. 16006–16026, 2021.

[26] P. Shahkarami and S. Fatemi, "Mathematical modeling and optimization of combined steam and dry reforming of methane process in catalytic fluidized bed membrane reactor," *Chemical Engineering Communications*, vol. 202, no. 6, pp. 774–786, 2015.

[27] Q. Yuan, R. Gu, J. Ding, and J. Lu, "Heat transfer and energy storage performance of steam methane reforming in a tubular reactor," *Applied Thermal Engineering*, vol. 125, pp. 633–643, 2017.

[28] J. Chen and L. Li, "Thermal management of methanol reforming reactors for the portable production of hydrogen," *International Journal of Hydrogen Energy*, vol. 45, no. 4, pp. 2527–2545, 2020.

[29] P. Li, L. Chen, S. Xia et al., "Entropy generation rate minimization for steam methane reforming reactor heated by molten salt," *Energy Report*, vol. 6, pp. 685–697, 2020.

[30] V. A. Savelieva, N. S. Titova, and I. V. Arsentiev, "Numerical study of syngas production during partial oxidation of sour natural gases upon activation of oxygen by an electrical discharge," *Energy & Fuels*, vol. 33, no. 11, pp. 11887–11898, 2019.

[31] K. Pornmai, W. Ngamkala, T. Rirksomboon, P. Ouraipryvan, and S. Chavadej, "Re-forming of CO2-containing natural gas with steam and partial oxidation over Ni catalysts in corona discharge for synthesis gas production," *Industrial & Engineering Chemistry Research*, vol. 58, no. 16, pp. 6203–6217, 2019.

[32] L. Hoseinzade and T. A. Adams II, "Modeling and simulation of an integrated steam reforming and nuclear heat system," *International Journal of Hydrogen Energy*, vol. 42, no. 39, pp. 25048–25062, 2017.

[33] J. Jin, X. Wei, M. Liu et al., "A solar methane reforming reactor design with enhanced efficiency," *Applied Energy*, vol. 226, pp. 797–807, 2018.

[34] T. Xie, K.-D. Xu, Y.-L. He, K. Wang, and B.-L. Yang, "Thermodynamic and kinetic analysis of an integrated solar thermochemical energy storage system for dry-reforming of methane," *Energy*, vol. 164, pp. 937–950, 2018, dry.

[35] D. D. Nguyen, S. I. Ngo, Y.-I. Lim et al., "Optimal design of a sleeve-type steam methane reforming reactor for hydrogen production from natural gas," *International Journal of Hydrogen Energy*, vol. 44, no. 3, pp. 1973–1987, 2019.

[36] T. Yu, Q. Yuan, J. Lu, J. Ding, and Y. Lu, "Thermochemical storage performances of methane reforming with carbon dioxide in tubular and semi-cavity reactors heated by a solar dish system," *Applied Energy*, vol. 185, pp. 1994–2004, 2017.

[37] H. Wu, V. La Parola, G. Pantaleo, F. Puleo, A. Venezia, and L. Liotta, "Ni-based catalysts for low temperature methane steam reforming: recent results on Ni-Au and comparison with other Bi-metallic systems," *Catalysts*, vol. 3, no. 2, pp. 563–583, 2013.

[38] O. Shtyka, M. Zakrzewski, R. Ciesielski et al., "Efficient removal of the carbon deposits formed during the mixed methane reforming over Ni/Al2O3," *Korean Journal of Chemical Engineering*, vol. 37, no. 2, pp. 209–215, 2020.

[39] M. H. A. Shiraz, M. Rezaei, and F. Meshkani, "The effect of promoters on the CO2 reforming activity and coke formation of nanocrystalline Ni/Al2O3 catalysts prepared by microemulsion method," *Korean Journal of Chemical Engineering*, vol. 33, no. 12, pp. 3359–3366, 2016.

[40] D. Zhang, G. Wei, Y. Wang et al., "Carbon dioxide reforming of methane over MgO promoted Ni/CNT catalyst," *Korean Journal of Chemical Engineering*, vol. 35, no. 10, pp. 1979–1987, 2018.

[41] R. Xu and T. F. Wiesner, "Dynamic model of a solar thermochemical water-splitting reactor with integrated energy collection and storage," *International Journal of Hydrogen Energy*, vol. 37, no. 3, pp. 2210–2223, 2012.

[42] C. N. R. Rao and S. Dey, "Solar thermochemical splitting of water to generate hydrogen," *Proceedings of the National Academy of Sciences*, vol. 114, no. 51, pp. 13385–13393, 2017.

[43] J. Miller, K. Nwe, Y. Youn et al., "Development of a low environmental impact, porous solar absorber coating utilizing binary/ternary solvent blends for CSP systems," *Korean Journal of Chemical Engineering*, vol. 36, no. 6, pp. 996–1003, 2019.

[44] S. A. M. Said, M. Waseeuddin, and D. S. A. Simakov, "A review on solar reforming systems," *Renewable and Sustainable Energy Reviews*, vol. 59, pp. 149–159, 2016.

[45] M. Böhmer, U. Langnickel, and M. Sancehz, "Solar Energy Materials," *Science Direct*, vol. 24, p. 441, 1991.

[46] A. Berman, R. K. Karn, and M. Epstein, “Steam reforming of methane on a Ru/Al2O3 catalyst promoted with Mn oxides for solar hydrogen production,” *Green Chemistry*, vol. 9, no. 6, p. 626, 2007.

[47] G. De Maria, L. D’Alessio, E. Coffari, M. Paolucci, and C. A. Tiberio, “Thermochemical storage of solar energy with high-temperature chemical reactions,” *Solar Energy*, vol. 35, no. 5, pp. 409–416, 1985.

[48] G. De Maria, C. A. Tiberio, L. D’Alessio, M. Piccirilli, E. Coffari, and M. Paolucci, “Thermochemical conversion of solar energy by steam reforming of methane,” *Energy*, vol. 11, no. 8, pp. 805–810, 1986.

[49] R. Buck, J. F. Muir, and R. E. Hogan, “Carbon dioxide reforming of methane in a solar volumetric receiver/reactor: the CAESAR project,” *Solar Energy Materials*, vol. 24, no. 1-4, pp. 449–463, 1991.

[50] J. F. Muir, R. E. Hogan, R. D. Skocypec, and R. Buck, “Solar Energy Materials,” *Science Direct*, vol. 5, p. 466, 1994.

[51] R. D. Skocypec, R. E. Hogan Jr., and J. F. Muir, “Solar reforming of methane in a direct absorption catalytic reactor on a parabolic dish: II-Modeling and analysis,” *Solar Energy*, vol. 52, no. 6, pp. 479–490, 1994.

[52] M. De Falco and V. Piemonte, “Solar enriched methane production by steam reforming process: reactor design,” *International Journal of Hydrogen Energy*, vol. 36, no. 13, pp. 7759–7762, 2011.

[53] J. Jia, L. C. Seitz, J. D. Benck et al., “Solar water splitting by photovoltaic-electrolysis with a solar-to-hydrogen efficiency over 30%,” *Nature Communications*, vol. 7, no. 1, p. 13237, 2016.

[54] F. Gallucci, E. Fernandez, P. Corengia, and M. van Sint Annaland, “Recent advances on membranes and membrane reactors for hydrogen production,” *Chemical Engineering Science*, vol. 92, pp. 40–66, 2013.

[55] S. Uemiya, N. Sato, H. Ando, T. Matsuda, and E. Kikuchi, “Steam reforming of methane in a hydrogen-permeable membrane reactor,” *Applied Catalysis*, vol. 67, no. 1, pp. 223–230, 1990.

[56] F. A. N. Fernandes and A. B. Soares Jr., “Methane steam reforming modeling in a palladium membrane reactor,” *Fuel*, vol. 85, no. 4, pp. 569–573, 2006.

[57] D. S. A. Simakov and M. Sheintuch, “Model-based optimization of hydrogen generation by methane steam reforming in autothermal packed-bed membrane reformer,” *AIChE Journal*, vol. 57, no. 2, pp. 525–541, 2011.

[58] P. Marín, Y. Patino, F. V. Díez, and S. Ordónez, “Catalyst deactivation in the direct synthesis of dimethyl ether from syngas over CuO/ZnO/Al2O3 and □-Al2O3 mechanical mixtures,” *International Journal of Hydrogen Energy*, vol. 37, Article ID 18433, 2012.

[59] W. Fuqiang, C. Ziming, T. Jianyu, Y. Yuan, S. Yong, and L. Linhua, “Progress in concentrated solar power technology with parabolic trough collector system: a comprehensive review,” *Renewable and Sustainable Energy Reviews*, vol. 79, pp. 1314–1328, 2017.

[60] D. S. A. Simakov, M. M. Wright, S. Ahmed, E. M. A. Mokheimer, and Y. Román-Leshkov, “Solar thermal catalytic reforming of natural gas: a review on chemistry, catalysis and system design,” *Catalysis Science & Technology*, vol. 5, no. 4, pp. 1991–2016, 2015.

[61] A. Steinfeld, “Solar thermochemical production of hydrogen--a review,” *Solar Energy*, vol. 78, no. 5, pp. 603–615, 2005.

[62] C. Agrafiotis, H. von Storch, M. Roeb, and C. Sattler, “Solar thermal reforming of methane feedstocks for hydrogen and syngas production-A review,” *Renewable and Sustainable Energy Reviews*, vol. 29, pp. 656–682, 2014.

[63] K. P. M. de Lima, V. da Fonseca Dias, and J. D. da Silva, *International Journal of Hydrogen Energy*, vol. 45, p. 10353, 2020.

[64] D. Yadav and R. Banerjee, “Lipid reducing potential of liposomes loaded with ethanolic extract of purple pitanga (Eugenia uniflora) administered to Caenorhabditis elegans,” *Renewable and Sustainable Energy Reviews*, vol. 54, pp. 497–532, 2016.

[65] H. Wang, Y. Hao, and H. Kong, “Thermodynamic study on solar thermochemical fuel production with oxygen permeation membrane reactors,” *International Journal of Energy Research*, vol. 39, no. 13, pp. 1790–1799, 2015.

[66] S. A. M. Said, D. S. A. Simakov, E. M. A. Mokheimer et al., “Computational fluid dynamics study of hydrogen generation by low temperature methane reforming in a membrane reactor,” *International Journal of Hydrogen Energy*, vol. 40, no. 8, pp. 3158–3169, 2015.

[67] S. A. M. Said, D. S. A. Simakov, M. Waseeuddin, and Y. Román-Leshkov, “Solar molten salt heated membrane reformer for natural gas upgrading and hydrogen generation: a CFD model,” *Solar Energy*, vol. 124, pp. 163–176, 2016.

[68] V. Pranesh, R. Velraj, S. Christopher, and V. Kumaresan, “A 50 year review of basic and applied research in compound parabolic concentrating solar thermal collector for domestic and industrial applications,” *Solar Energy*, vol. 187, pp. 293–340, 2019.

[69] B. Lee, S.-W. Yun, S. Kim et al., “CO2 reforming of methane for H2 production in a membrane reactor as CO2 utilization: computational fluid dynamics studies with a reactor geometry,” *International Journal of Hydrogen Energy*, vol. 44, no. 4, pp. 2298–2311, 2019.

[70] R. B. Bird, W. E. Stewart, E. N. Lightfoot, New York, John Wiley & Sons 1960.

[71] S. Lee and H. Lim, “Advances and challenges in electrochemical CO2 reduction processes: an engineering and design perspective looking beyond new catalyst materials,” *Journal of Industrial and Engineering Chemistry*, vol. 87, p. 110, 2020.

[72] J. T. Richardson and S. A. Paripatyadar, “Carbon dioxide reforming of methane with supported rhodium,” *Applied Catalysis*, vol. 61, no. 1, pp. 293–309, 1990.

[73] S. Lee and H. Lim, “The power of molten salt in methane dry reforming: conceptual design with a CFD study,” *Chemical Engineering and Processing - Process Intensification*, vol. 159, Article ID 108230, 2021.